ENGLISH VERSION..

Setting time and mechanical properties of alkali-activated ash/slag cements cured at room temperature

Tiempo de configuración y propiedades mecánicas de cementos de ceniza / escoria activados con álcali curados a temperatura ambiente

P. Caetano*[1] http://orcid.org/0000-0003-1845-2702
T. Batista * http://orcid.org/0000-0001-6598-0319
R. Nogueira* http://orcid.org/0000-0002-2000-4426
A. Cabral* http://orcid.org/0000-0001-6394-1164
H. Costa* http://orcid.org/0000-0001-9960-2383

* Federal University of Ceará, BRAZIL

Abstract

The focus of this paper is to investigate the behavior of the fresh and hardened state of alkali-activated cementitious pastes obtained from the mixture of bottom ash/BOF slag and fly ash/BOF slag. For this purpose, the properties in the fresh and hardened state were evaluated. Ten pastes were produced in two separate systems, whose proportions between ashes and BOF slag were 100:0, 75:25, 50:50, 25:75, and 0:100 (fly ash or bottom ash: BOF slag). In general, the addition of BOF steel slag works by accelerating the setting times, at room temperature curing. In addition, the stress-strain curves demonstrated that heavy ash and BOF steel slag favor the ductile behavior under axial stress. Furthermore, the addition of BOF slag can influence the properties in the fresh and hardened state. Therefore, it is feasible to use steel slag combined with coal ash in alkaline activated binary mixtures.

Keywords: Alkali-activated; cement; acceleration curing; physical properties; mechanical properties.

Resumen

El objetivo de este trabajo es investigar el comportamiento del estado fresco y endurecido de las pastas cementosas activadas con álcali obtenidas de la mezcla de cenizas de fondo/escoria BOF y cenizas volantes/escoria BOF. Para el propósito, se evaluaron las propiedades en el fresco y estado endurecido. Se produjeron diez pastas en dos sistemas separados, cuyas proporciones entre cenizas y escoria BOF fueron 100: 0, 75:25, 50:50, 25:75 y 0: 100 (cenizas volantes o cenizas de fondo: escoria BOF). En general, la adición de escoria de acero BOF actúa acelerando los tiempos de configuración, a temperatura ambiente de curado. Además, las curvas tensión-deformación demostraron que las cenizas pesadas y la escoria de acero BOF favorecen el comportamiento dúctil en tensión axial. Además, la adición de escoria BOF puede influir en las propiedades en estado fresco y endurecido. Por tanto, es factible utilizar escoria de acero combinada con ceniza de carbón en mezclas binarias alcalinas activadas.

Palabras clave: Alcalino-activado; cemento; curado de la aceleración; propiedades físicas; propiedades mecánicas.

[1] Corresponding author:
Federal University of Ceará, BRAZIL
E-mail: phablo.caetano@gmail.com

1. Introduction

Alkali-activated cements are composed of powdered materials, which are rich in aluminosilicates mixed in an alkaline solution. The precursor materials can be natural or residual from other industrial processes. They are divided into two groups: a group of precursors with low calcium content, represented by metakaolin and fly ash; and a group of precursors with high calcium content, represented by blast furnace slag (Provis and Van Deventer, 2014).

The use of alkali-activated cements based on blast furnace slag and fly ash has been indicated in the literature for the production of pastes, mortars and concretes(Provis, 2018); (NG et al., 2018)). In general, alkali-activated cements have high mechanical strength, adequate durability, and environmental benefits due to the low emission of carbon dioxide (CO_2) in the production process (Zhou et al., 2020). However, alkali-activated materials based on low calcium ash require heat treatment to accelerate chemical reactions and gain strength, which makes their on-site application difficult (Guo et al., 2010); (Pavithra et al., 2016).

For this reason, there has been an investment in binary cement fly ash/blast furnace slag to promote the application at room temperature (Lee and Lee, 213); (Nath and Kumar, 2017); (Dhing et al., 2018); (Aboulayt et al., 2020). Moreover, fly ash and blast furnace slag are value-added by-products since a large portion of them are used as supplementary material in cement industries (Provis and Van Deventer, 2014). Bottom ash and basic oxygen furnace (BOF) steel slag are also by-products generated in coal-based thermoelectric energy and steelmaking industries, respectively. In addition to low reactivity, these residues have granulometries that vary between coarse and fine aggregates, making it difficult to reuse them to form cementitious materials (Topçu et al., 2014); (Naidu et al., 2020).

Bottom ash accounts for between 10% and 20% of the total residual from the combustion of coal in thermoelectric plants (Ul Haq et al., 2014). Usually, they are accumulated in landfills that do not have a defined destination (Xie and Ozbakkaloglu, 2015). Furthermore, the use of BOF slag is an environmental challenge due to the large volume of material that is produced annually and its potentially harmful environmental impacts (Naidu et al., 2020). It is estimated that between 200 and 250 kg of BOF slag are generated per ton of steel produced, and they are usually discarded due to the presence of metals and expansive behavior (Kumar et al., 2019).

In terms of chemical composition, bottom ash is similar to fly ash, the biggest difference is in the particle size (Santa et al., 2013). Recently, some studies have been developed with the use of bottom ash combined with other precursors in binary cements. The studies aimed at optimizing the results since bottom ash has lower mechanical strength compared to fly ash (Boonserm et al., 2012); (Li et al., 2012); (Kumar and Revathi, 2016); (Santa et al., 2016); (Kalaw et al., 2016); (Hanjitsuwan et al., 2017). However, there is little research on BOF slag and its use as a precursor of alkali-activated cement (Naidu et al., 2020). An incipient study by (Gevaudan et al., 2018) used BOF slag in a composition of metakaolin in alkali-activated cement, micro-doped with copper and cobalt. The goal of the study was to investigate the resistance to attack by acids.

The use of BOF slag in binary cement with fly ash and bottom ash extends the investigation of this type of slag behavior in alkali-activated materials. Moreover, this use of BOF slag can enable the recycling of waste without a destination, adding value to them and generating new products for the civil construction industry. Therefore, this paper aims to investigate the behavior in the fresh and hardened state of alkali-activated cementitious pastes obtained from the mixture of bottom ash/BOF slag and fly ash/BOF slag. To this end, this investigation evaluated the setting time and spreading in the mini-slump, in the fresh state; and the compressive strength, stress-strain curve, elastic modulus, and fracture energy, in the hardened state.

2. Materials and methods

Fly ash and bottom ash came from the Thermoelectric Power Plant at Pecém, state of Ceará, Brazil. The BOF steel slag originated from Pecém Steel Company, state of Ceará. The chemical characterization performed by X-ray fluorescence (FRX) provided the percentages of the main oxides in the precursors, as shown in (Table 1). Physical characteristics such as maximum particle size and specific surface area obtained by laser diffraction were also presented.

Table 1. Chemical and physical characteristics of precursors

Components/ chemicals/physical characteristics	% Oxides		
	Fly ash	Bottom ash	BOF slag
SiO_2	41,49	50,66	6,40
Al_2O_3	14,49	10,66	1,80

CaO	9,54	5,61	52,00
Fe_2O_3	24,95	26,99	34,30
K_2O	4,54	3,68	0,20
Others	4,96	0,63	5,3
Maximum dimension	30,506 μm	164,203 μm	158,993 μm
Specific surface area	17300 cm²/g	2750 cm²/g	5710 cm²/g
Density	2,18 g/cm³	1,52 g/cm³	2,92 g/cm³

The alkaline activator was composed of sodium hydroxide in micro-pearls with 97% and commercial sodium silicate. The sodium hydroxide solution was prepared with distilled water 24 hours in advance. Sodium silicate contains 15.08% of Na_2O and 32.69% of SiO_2, which are 47.77% of total solids, SiO_2/Na_2O ratio of 2.17, and density of 1.57 g/cm³.

3.   Mixing and tests performed

Pastes were grouped into two different systems: BB (bottom ash: BOF slag) and FB (fly ash: BOF slag). In both systems, the variation of BOF slag content was 0%, 25%, 50%, 75%, and 100%. In the BB system, the selected alkaline solution/binder (a/b) ratio was 0.6, and the molar concentration of sodium hydroxide (M) was 8 mol/l. In the FB system, the a/b ratio was 0.5, and M was 16 mol/l. However, the relationship between sodium silicate and sodium hydroxide was fixed at 1.

Initially, the components were pre-homogenized manually for 1 minute. Next, we used the planetary mixer for 1 minute, performing a pause. Finally, the mechanical mixing was completed for another 2 minutes. After mixing, the measurement of the spreading diameter was carried out in the mini-slump test (Kantro, 1980). Also, the initial setting time and end setting time were performed according to the specifications of NBR 16607 (ABNT,2018). The setting speed was calculated according to (Equation 1).

$$S = \frac{P}{t_{10}-t_4}$$
(1)

Where: P is the constant penetration distance (6 mm); S is the setting speed (mm/min); t_{10} is the time until the needle reaches a penetration resistance equal to 10 mm, and t_4 is the time until the needle reaches a penetration resistance equal to 4 mm.

Specimens measuring 40 mm x 40 mm x 40 mm were produced for the compressive strength tests at 7 and 28 days. Curing was conducted at room temperature up to the age of rupture. During the compressive strength tests, the displacements of every second were also recorded by means of transducers built into the equipment, which made it possible to trace the stress-strain curve of the samples. With the data from the curves, the elastic modulus was calculated according to (Equation 2), according to NBR 8522 (ABNT,2017). In addition, the fracture energy was obtained according to (Equation 3) (Bazant et al., 2002).

$$E = \frac{\sigma-0,5}{\varepsilon-\varepsilon_{0,5}}$$
(2)

$$G_{f=2,5*\alpha 0*(\frac{fc}{0,051})^{0,46}*(1+\frac{D_{máx}}{11,27})^{0,22}*(\frac{a}{b})^{-0,30}}$$
(3)

Where: E is the elastic modulus (GPa); σ is the tension corresponding to 30% of the compressive strength, ε is the deformation referring to σ; $\varepsilon_{0,5}$ is the deformation corresponding to 0,5 MPa; G_f is the fracture energy (N/m); $D_{máx}$ is the maximum particle size (mm); f_c is the average compressive strength (MPa); a/b is the alkaline solution/binder ratio; α0 =1 for rounded particles (fly ash), and α0= 1,44 for angular particles (bottom ash and BOF slag).

4.   Results and discussion

Setting time and workability

The mini-slump results for the BB and FB systems can be seen in (Figure 1).
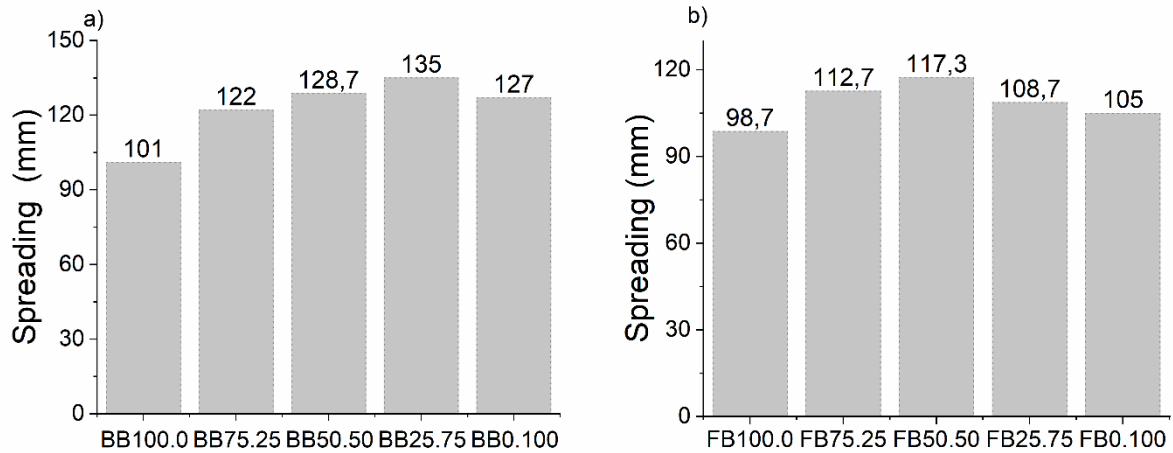
Figure 1. Mini-slump spread: a) BB system; b) FB system

As shown in (Figure 1a), the BB25:75 paste presented better workability in the BB system, obtaining the largest spreading diameter. The higher percentage of bottom ash influenced the behavior of the pastes, making them less fluid. On the other hand, BB0:100 paste (100% BOF slag) showed a smaller spreading diameter compared to BB50:50 and BB25:75 pastes. As shown in (Figure 1b), the FB50:50 paste presented the best workability in the FB system, whose spreading diameter was 117.3 mm, showing more fluid characteristics. Thus, the combination of smaller particles of fly ash and larger particles of BOF steel slag probably favored workability, which made the voids left by larger particles be filled with smaller particles, improving particle packing (Sathonsaowaphak et al., 2009). On the other hand, the FB100:0 paste showed the least fluid behavior. This sample is composed of 100% fly ash, which has a high specific surface area, as seen in (Table 1). Therefore, the lower workability is related to the higher demand for activating solutions so that particles can be enveloped (Campos et al., 2019).

In addition to determining the initial and final time of setting, the evolution (difficulty) of needle penetration overtime was also monitored and was called penetration resistance. The results for the BB and FB systems are shown in (Figure 2a) and (Figure, 2b), respectively.
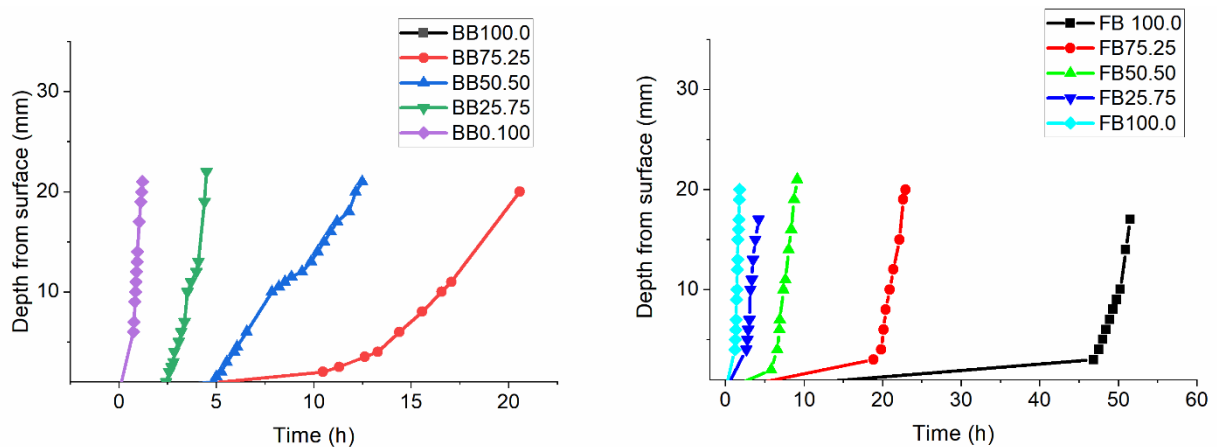
Figure 2. Evolution of setting time: a) BB system; b) FB system

In the BB system (Figure 2a), the BB0:100 paste took 45 minutes to reach a penetration resistance equal to 6 mm and around 1 hour and 52 minutes to reach the end setting time (Figure 3a). Meanwhile, the folders with an

increment of bottom ash had longer setting times. The BB100:0 sample (100% bottom ash) did not register the initial setting time until 120h of testing, and for this reason, it is not present in (Figure 2a).

In the FB system, the VB0:100 paste (100% BOF slag) recorded the shortest setting times, reaching the beginning of setting time in about 1.3 hours (Figure 2a) and the end of setting around 5.45 hours (Figure 3b). The paste with 100% fly ash (PB100:0) took 48.4 hours to start setting. However, an important change can be observed in the PB75:25 paste, where the incorporation of only 25% of BOF slag allowed the start of setting to occur within 14.4 hours after mixing.
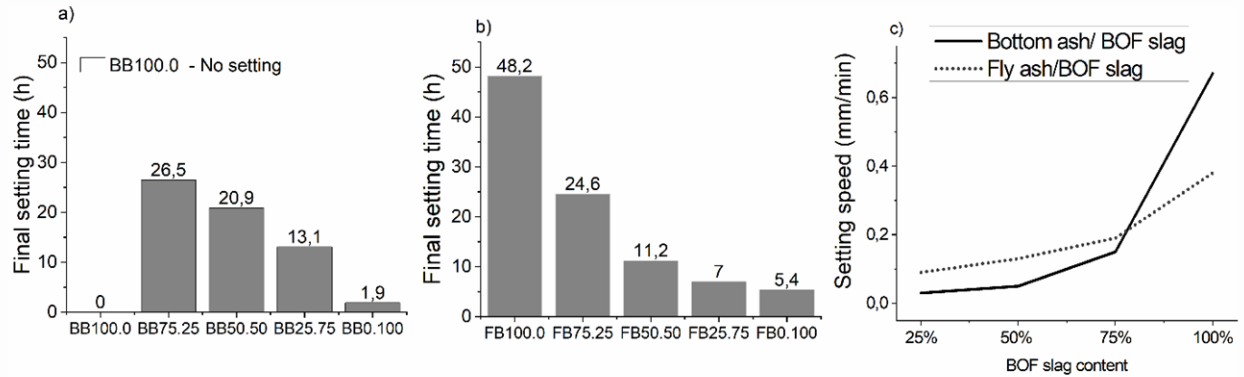
Figure 3. *a) Final setting time of BB system; b) Final setting time of FB system; c) influence of BOF slag on setting*

In both systems, the higher the percentage of BOF slag, the faster the start and end of the setting time occur. Therefore, this precursor acts as a setting accelerator. This behavior was also observed by (Lee and Lee, 2013) and is generally related to the increase in the content of CaO, the main chemical component of BOF slag (Table 1), which accelerates the hydration reaction of the mixture. This directly influences the setting time of the paste (Wijaya et al., 2017), as it acts aiding dissolution of aluminosilicate and accelerating reactions (Canfield et al., 2014). The accelerated setting time also affects workability, as the paste decreases flow over time. In (Figure 3c), the setting speed of pastes changes over time. For both the BB system and the FB system, the increase in the amount of BOF slag in the mixtures caused a higher setting speed. This behavior was expected and is in agreement with the literature (Lee and Lee, 2013); (Canfield et al., 2014); (Hadi et al., 2017).

5. *Mechanical properties*

The compressive strengths at 7 and 28 days of the BB and FB systems are shown in (Figure 4a) and (Figure 4b), respectively.
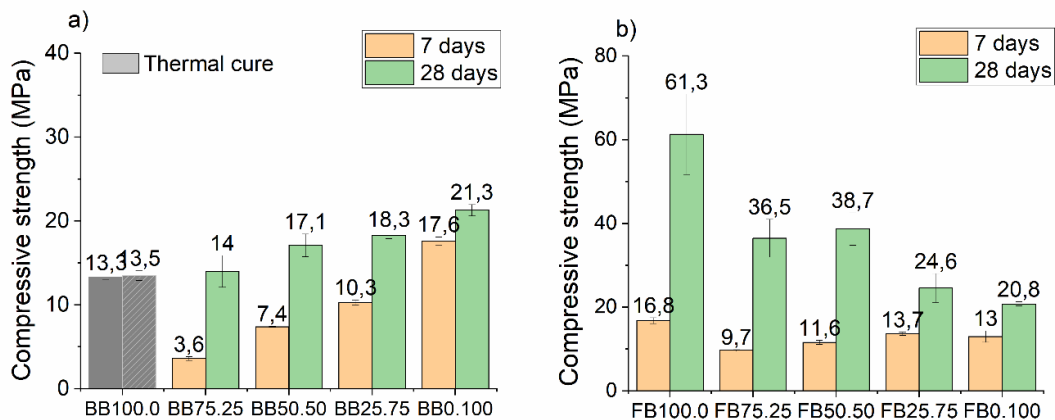
Figure 4. *Compressive strength: a) BB system; b) FB system*

The BB100:0 paste (100% bottom ash), highlighted in (Figure 4a), was thermally cured at 80°C, reaching a strength of 13.30 MPa after 7 days. This paste received thermal cure due to the non-occurrence of the beginning of setting time verified in the previous topic. In (Figure 4a), the addition of BOF slag in the BB system promoted an increase in compressive strength, registering an increase at 28 days for the pastes with 25%, 50%, and 75% slag, and with 14 MPa, 17.11 MPa, and 18.34 MPa, respectively. This behavior agrees with the studies by (Aziz et al., 2017) and (Liu et al., 2018) that indicate that precursors with higher contents of CaO can significantly interfere in the compressive strength gain of alkali-activated pastes. The bottom ash was considered less reactive in alkali-activated materials because of the large particles and irregular shape with pores and cavities (Ul Haq et al., 2014).

However, in the FB system (Figure 4b), the addition of BOF slag caused a reduction in strength. In this system, the best performances were observed in the pastes with the highest levels of fly ash. The FB100:0 paste (100% fly ash) obtained greater compressive strength (61.3 MPa) at 28 days. At this age, the pastes with 25% and 50% BOF slag reached 36.5 and 38.7 MPa, respectively. From 75% BOF slag, the strengths were less than 25 MPa. This behavior was also consistent since fly ash is a recognized precursor for the most suitable chemical and physical characteristics for alkali activation, providing better physical and mechanical properties (Khale and Chaudhary, 2007); (Fernández-Jiménez and Palomo, 2003). (Figure 5a) and (Figure 5b) showed the stress-strain curves of the BB and FB systems, respectively. For each paste, the curves of the 03 test specimens tested were presented.
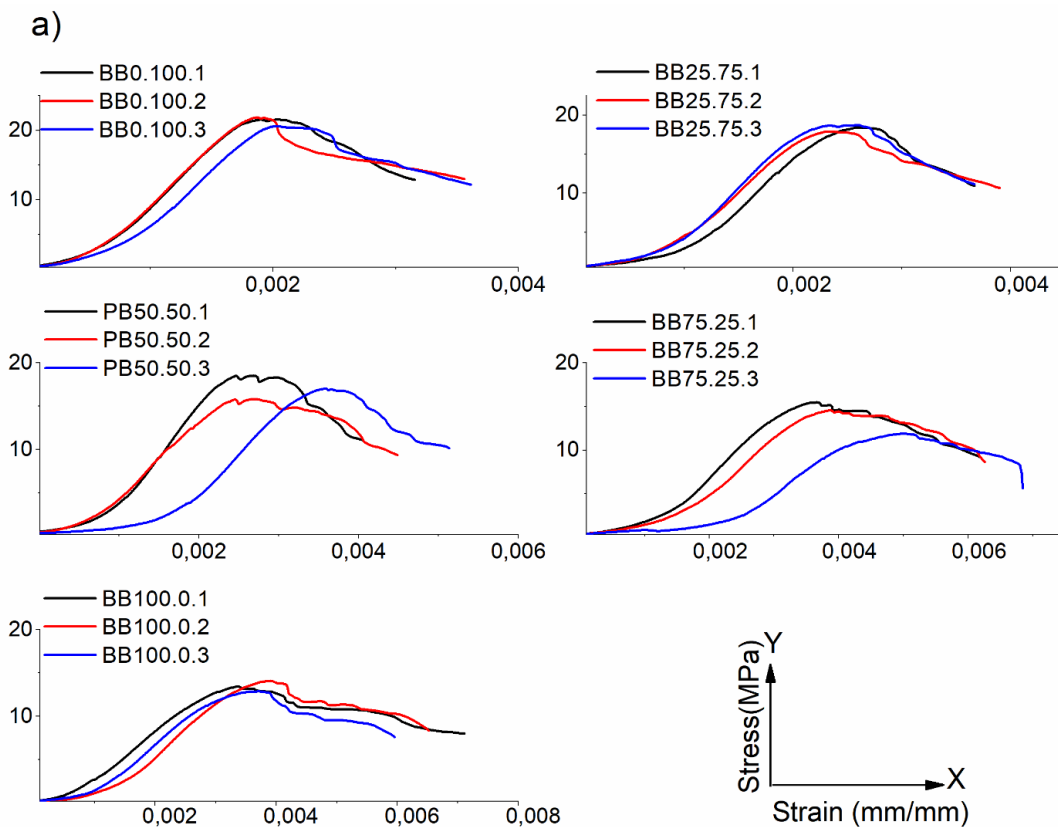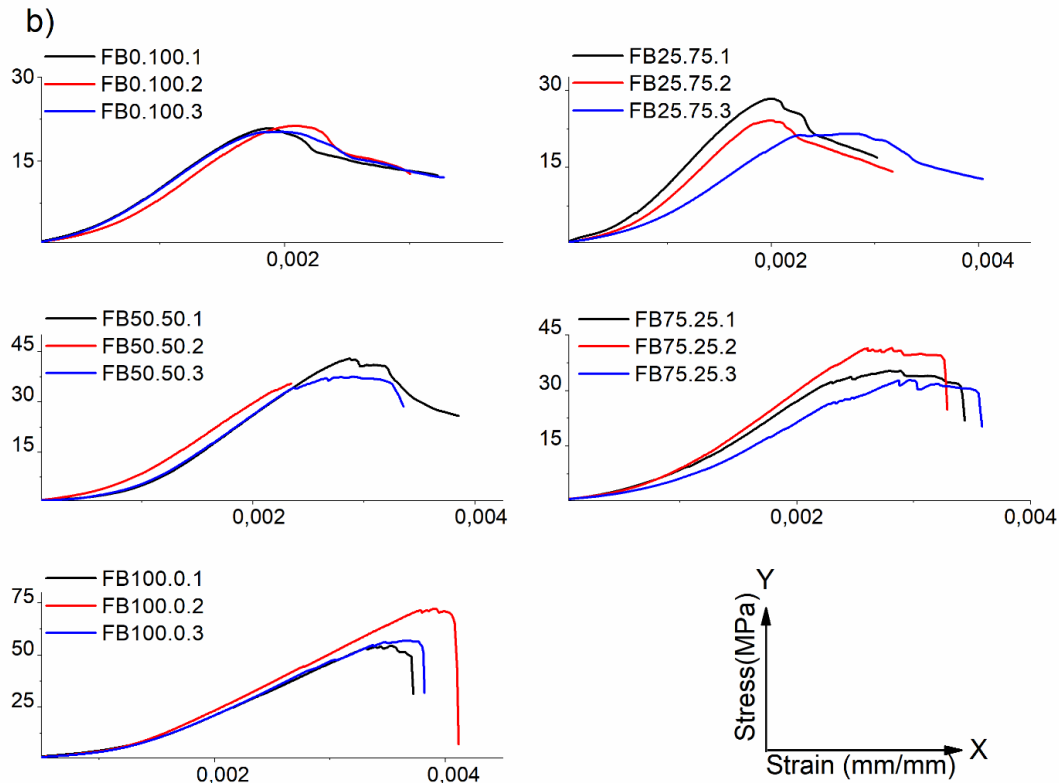
Figure 5. *Stress-strain curves: a) BB system; b) FB system*

The stress-strain curves of the pastes in the BB system (Figure 5a) presented elongated post-peak curves. There were greater deformations in the pastes with higher contents of bottom ash, both before and after the resistance peak. In the FB system curves (Figure 5b), the descending branches got more accentuated as higher levels of BOF slag were being added. In FB100:0 paste (100% fly ash) the descending branch showed a steep curvature, indicating greater fragility of this paste (Figure 5b).

In general, the behavior of the stress-strain curves demonstrated that bottom ash and BOF steel slag favor the more ductile behavior under axial stress. To complement the analysis, Figures 6a and 6b presented the estimated fracture energy of the BB and FB systems, respectively. The fracture characteristics of a material are used to describe the formation and propagation of its cracks and to reflect the fragility and response of the material under stress (Ding et al., 2016). Paste is one of the determinants of fracture energy in Portland cement and activated alkaline cement-based materials (Pan et al., 2011).
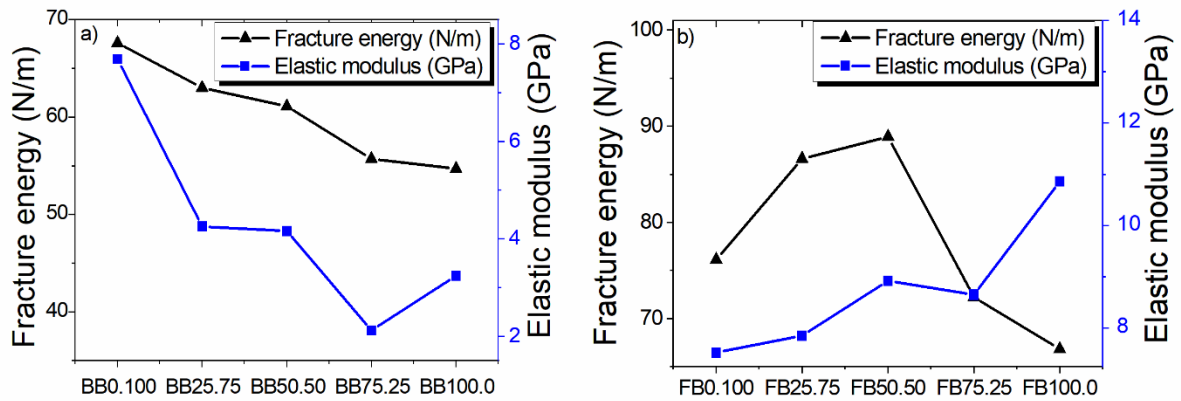
Figure 6. Fracture energy and elastic modulus: a) BB system; b) FB system

According to the prediction model used (Equation 3), in the BB system, the highest fracture energy was observed in the paste with 100% BOF slag (BB0:100), decreasing with higher contents of bottom ash. On the other hand, in the FB system, the highest fracture energies were observed in the FB75:25 and FB50:50 pastes. Meanwhile, the lowest energy was observed in the FB100:0 paste (100% fly ash). Lower fracture energy values indicated a fragile behavior during rupture, corroborating the aspect observed in (Figure 5b.e), in which the load-deflection branch was more intense, and that is common for abrupt ruptures. On the other hand, higher values of fracture energy indicate more ductile behavior of the material (Nath and Kumar, 2017).

The elastic modulus of the pastes is shown in (Figure 6a) and (Figure 6b). For the BB system, a more elastic behavior was seen in pastes with higher contents of bottom ash. In the FB system, the elastic modulus was lower for the pastes with lower BOF slag contents, indicating more flexible pastes. Therefore, the influence that the type of precursor has on the elastic modulus was noted according to (Ding et al., 2018), who state that the type of precursor is one of the factors that influence the elastic modulus of the paste, due to the characteristics of the microstructure developed.

6. Conclusions

Ten alkali-activated pastes based on coal ash and BOF slag were tested in the fresh state to evaluate setting times and spreading in the mini-slump. Additionally, the compressive strength test was performed, and the stress-strain curves, elastic modulus, and fracture energy were analyzed. The pastes were divided into two binary systems: BB (bottom ash: BOF slag) and FB (fly ash: BOF slag); varying the BOF slag content in 0%, 25%, 50%, 75%, and 100%. In summary, the main conclusions of the study are the following:

- The workability of the pastes, both in the BB system and in the FB system was improved in mixtures between 25% and 75% of BOF slag, depending on the granulometric composition of the two precursors of each system;
- The incorporation of BOF slag in the BB system promoted initial setting times of 14.4 h, 6.56 h, and 3.2 h, with the addition of 25%, 50%, and 75%, respectively. Similar behavior was observed in the FB system, which obtained initial setting time around 20.13 h, 6.87 h, and 2.88 h, with the addition of 25%, 50%, and 75% of BOF slag. Thus, the higher the BOF slag content, the lower the setting time of binders. Therefore, BOF steel slag acted as a setting accelerator in both systems;
- The compressive strength at 28 days of the PB system increased with the percentage increase of BOF slag, reaching values equal to 14.00 MPa, 17.11 MPa, and 18.34 MPa, with the addition of 25%, 50%, and 75% BOF slag, respectively. However, an opposite effect was observed in the FB system in composition with fly ash. The increase of 25%, 50%, and 75% of BOF slag resulted in strengths of 36.5 MPa, 38.7 MPa, and 24.6 MPa, respectively. These values were lower to the sample with 100% fly ash (61.3 MPa);
- The behavior observed in the stress-strain curves demonstrates that bottom ash and BOF steel slag favor the ductile behavior under axial stress. In the FB system, the FB100:0 paste curve indicated greater fragility of the sample with 100% fly ash. This was confirmed by the low fracture energy of this sample since lower fracture energy values indicate a fragile behavior at rupture;
- Pastes with higher contents of bottom ash in the BB system and with higher contents of BOF slag in the FB system have lower values of elastic modulus; therefore, they tend to be more flexible.

Briefly, the addition of BOF steelmaking slag influences the properties of fresh and hardened cement pastes based on the coal ash. Therefore, in the correct proportion, the addition of slag can positively influence workability and compressive strength. Moreover, it acts as a setting accelerator, which directly influences the feasibility of the application of cements at room temperature. Thus, it is feasible to use BOF slag combined with coal ash, and further investigations into the application of these cements in composites for civil construction are recommended.

7.   Acknowledgements

8.   References

ABNT (Associação Brasileira de Normas Técnicas). (2018). *NBR 16607 - Portland cement - Determination of setting times". Rio de Janeiro.*

ABNT (Associação Brasileira de Normas Técnicas). (2017). *NBR 8522 - Concrete - Determination of static modulus of elasticity and deformation by compression. Rio de Janeiro.*

Aboulayt, A., Souayfan, F., Roziere, E., Jaafri, R., Idrissi, AC., Moussa, R., Justino, C., Loukili, A. (2020). *Alkali-activated grouts based on slag-fly ash mixtures: From early-age characterization to long-term phase composition. Constr. Build. Mater, 260:120510, https://doi.org/10.1016/j.conbuildmat.2020.120510*

Aziz, IH., Zulkifly, K., Sakkas, K., Panias, D. Tsaousi, GM., Al Bakri, MMA., Yong, H. (2017). *The Characterization of Steel Slag by Alkali Activation. OALib, 4:1–13. https://doi.org/10.4236/oalib.1103816*

Bazant, Zdenek P., Becq-Giraudon, E. (2002). *Statistical prediction of fracture parameters of concrete and implications for choice of testing standard. Cem Concr Res, 32: 529–556.*

Boonserm, K., Sata, V., Pimraksa, K., Chindaprasirt, P. (2012). *Improved geopolymerization of bottom ash by incorporating fly ash and using waste gypsum as additive. Cem Concr Comp, 34:819–824, http://dx.doi.org/10.1016/j.cemconcomp.2012.04.001*

Campos, HF.; Rocha, TMS., Reus, GC., Klein, N.S., Marques Filho, J. (2019). *Determination of the optimal replacement content of Portland cement by stone powder using particle packing methods and analysis of the influence of the excess water on the consistency of pastes. Revista IBRACON de Estruturas e Materiais, 12:210–32, https://doi.org/10.1590/S1983-41952019000200002*

Canfield, GM., Eichler, J., Griffith, K., Hearn, JD. (2014). *The role of calcium in blended fly ash geopolymers. Journal of Materials Science, 49:5922–5933, DOI 10.1007/s10853-014-8307-z*

Chindaprasirt, P., Jaturapitakkul, C., Chalee, W., Rattanasak, U. (2009). *Comparative study on the characteristics of fly ash and bottom ash geopolymers. Waste Management, 29:539–543. doi:10.1016/j.wasman.2008.06.023*

Ding, Y., Dai, JG., Shi, CJ. (2016). *Mechanical properties of alkali-activated concrete: A state-of-the-art review. Constr. Build. Mater, 127:68–79, http://dx.doi.org/10.1016/j.conbuildmat.2016.09.121*

Ding, Y., Shi, C., Li, N. (2018). *Fracture properties of slag / fly ash-based geopolymer concrete cured in ambient temperature. Constr. Build. Mater, 190:787–795, https://doi.org/10.1016/j.conbuildmat.2018.09.138*

Fernández-Jiménez, A., Palomo, A. (2003). *Characterisation of fly ashes. Potential reactivity as alkaline cements. Fuel 82:2259–2265. doi:10.1016/S0016-2361(03)00194-7*

Gevaudan, JP., Caicedo-Ramirez, A., Hernandez, MT., Srubar III, WV. (2018). *Copper and cobalt improve the acid resistance of alkali-activated cements. Cem Concr Res, 115:327–338, https://doi.org/10.1016/j.cemconres.2018.08.002*

Guo, X., Shi, H., Dick, WA. (2010). *Compressive strength and microstructural characteristics of class C fly ash geopolymer. Cem Concr Comp, 32:142–147, doi:10.1016/j.cemconcomp.2009.11.003*

Hadi, MNS., Farhan, NA., Sheikh, MN, (2017), *Design of geopolymer concrete with GGBFS at ambient curing condition using Taguchi method. Constr. Build. Mater, 140:424–431, http://dx.doi.org/10.1016/j.conbuildmat.2017.02.131*

Hanjitsuwan, S., Phoo-Ngernkham, T., Damrongwiriyanupap, N. (2017). *Comparative study using Portland cement and calcium carbide residue as a promoter in bottom ash geopolymer mortar. Constr. Build. Mater, 133:128–134. http://dx.doi.org/10.1016/j.conbuildmat.2016.12.046*

Kalaw, ME., Culaba, A., Hinode, H., Kurniawan, W., Gallardo, S. Promentilla, MA. (2016). *Optimizing and characterizing geopolymers from ternary blend of philippine coal fly ash, coal bottom ash and rice hull ash. Materials, 9:7, doi:10.3390/ma9070580*

Kantro, D. (1980). *Influence of Water-Reducing Admixtures on Properties of Cement Paste—A Miniature Slump Test. Cement. Concrete and Aggregates 2:95.*

Khale, D., Chaudhary, R. (2007). *Mechanism of geopolymerization and factors influencing its development: A review. J. Mater. Sci, 42:729–746. DOI 10.1007/s10853-006-0401-4*

Kumar, DS., Sah, R., Sanyal, S., Prasad, G. (2019). *Measurement of metallic iron in steel making slags. Measurement, 131:156–161, https://doi.org/10.1016/j.measurement.2018.08.066*

Kumar, ML., Revathi, V. (2016). *Metakaolin bottom ash blend geopolymer mortar - A feasibility study. Constr. Build. Mater, 114:1–5. http://dx.doi.org/10.1016/j.conbuildmat.2016.03.149*

Lee, N. K., Lee, H. K. (2013). *Setting and mechanical properties of alkali-activated fly ash/slag concrete manufactured at room temperature. Constr. Build. Mater, 47:1201–1209, http://dx.doi.org/10.1016/j.conbuildmat.2013.05.107*

Li, Q., Xu, H., Li, F., Li, P., Shen, L., Zhai, J. (2012). *Synthesis of geopolymer composites from blends of CFBC fly and bottom ashes. Fuel, 97:366–372, doi:10.1016/j.fuel.2012.02.059*

Liu, B., Yang, J., Li, D., Xing, F., Fang, Y. (2018). *Effect of a synthetic nano-CaO-Al$_2$O$_3$-SiO$_2$-H$_2$O gel on the early-stage shrinkage performance of alkali-activated slag mortars. Materials, 11:7. doi:10.3390/ma11071128*

Naidu, TS., Sheridan, CM., Van Dyk, LD. (2020). *Basic oxygen furnace slag: Review of current and potential uses. Minerals Engineering, 149:106234. https://doi.org/10.1016/j.mineng.2020.106234*

Nath, P., Kumar, P. (2017). *Fracture properties of GGBFS-blended fly ash geopolymer concrete cured in ambient temperature. Mater Struct, 50:1–12, DOI 10.1617/s11527-016-0893-6*

NG, C., Alengaram, J., Wong,LS., Mo,K.H., Jumaat, M.Z., Ramesh, S. (2018). *A review on microstructural study and compressive strength of geopolymer mortar, paste and concrete. Constr. Build. Mater, 186: 550-576, https://doi.org/10.1016/j.conbuildmat.2018.07.075*

Pan, Z., Sanjayan, JG., Rangan, V. (2011). *Fracture properties of geopolymer paste and concrete. Magazine of concrete research, 63, 763–771. http://dx.doi.org/10.1680/macr.2011.63.10.763*

Pavithra, P., Reddy, M., Dinakar, P., Rao, BH, Satpathy, BK., Mohanty, AN. (2016). *A mix design procedure for geopolymer concrete with fly ash. J. Cleaner Prod, 133:117–125, http://dx.doi.org/10.1016/j.jclepro.2016.05.041*

Provis, J. L. (2018). *Alkali-activated materials. Cem Concr Res, 114:40-48: http://dx.doi.org/10.1016/j.cemconres.2017.02.009*

Provis, J. L.; Van Deventer, J. S. J. (2014) *Alkali-Activated Materials. State-of-the-Art Report, RILEM TC 224-AAM.*

Santa, RAAB., Soares, C., Riella, HG. (2016). *Geopolymers with a high percentage of bottom ash for solidification/immobilization of different toxic metals. J. Hazard. Mater, 318:145–153. http://dx.doi.org/10.1016/j.jhazmat.2016.06.059*

Santa, RAB., Bernandin, AM., Riella, HG., Kuhnen, NC. (2013). *Geopolymer synthetized from bottom coal ash and calcined paper sludge. J. Cleaner Prod, 57:302–307, http://dx.doi.org/10.1016/j.jclepro.2013.05.017*

Sathonsaowaphak, A., Chindaprasirt, P., Pimraksa, K. (2009). *Workability and strength of lignite bottom ash geopolymer mortar. J. Hazard. Mater, 168:44–50, doi:10.1016/j.jhazmat.2009.01.120*

Topçu, IB., Toprak, MU., Uygunoğlu, T. (2014). *Durability and microstructure characteristics of alkali activated coal bottom ash geopolymer cement. J. Cleaner Prod, 81:211–217. http://dx.doi.org/10.1016/j.jclepro.2014.06.037*

Ul Haq, E., Padmanabhan, SK., Licciulli, A. (2014). *Synthesis and characteristics of fly ash and bottom ash based geopolymers-A comparative study. Ceram. Int, 40:2965–2971. http://dx.doi.org/10.1016/j.ceramint.2013.10.012*

Wijaya, AL., Ekaputri, JJ., Triwulan. (2017). *Factors influencing strength and setting time of fly ash based-geopolymer paste. MATEC Web of Conferences, 138, 01010.*

Xie, T., Ozbakkaloglu, T. (2015). *Behavior of low-calcium fly and bottom ash-based geopolymer concrete cured at ambient temperature. Ceram. Int, 41: 5945–5958. http://dx.doi.org/10.1016/j.ceramint.2015.01.031*

Zhou, S., Ma, C., Long, G., Xie, Y. (2020). *A novel non-Portland cementitious material: Mechanical properties, durability and characterization. Constr. Build. Mater, 238:117671, https://doi.org/10.1016/j.conbuildmat.2019.117671*